energies

MDPI

Article

Outdoor Performance of Organic Photovoltaics: Comparative Analysis

Alberto Dolara [1,*], Sonia Leva [1], Giampaolo Manzolini [1], Riccardo Simonetti [1] and Iacopo Trattenero [2]

[1] Department of Energy, Politecnico di Milano, Via Lambruschini 4, 20156 Milano, Italy; sonia.leva@polimi.it (S.L.); giampaolo.manzolini@polimi.it (G.M.); riccardo.simonetti@polimi.it (R.S.)
[2] Eni Renewable Energy, Magnetic Fusion and Material Science Research Center, Via Fauser 4, 28100 Novara, Italy; iacopo.trattenero@eni.com
* Correspondence: alberto.dolara@polimi.it; Tel.: +39-02-23993829

Abstract: Organic photovoltaic (OPV) solar cells represent an emerging and promising solution for low-cost clean energy production. Being flexible and semi-transparent and having significant advantages over conventional PV technologies, OPV modules represent an innovative solution even in applications that cannot be based on traditional PV systems. However, relatively low efficiencies, poor long-term stability, and thermal issues have so far prevented the commercialization of this technology. This paper describes two outdoor experimental campaigns that compared the operation of OPV modules with traditional PV modules—in particular crystalline silicon and copper–indium–selenium (CIS)—and assessed the OPV modules' power generation potential in vertical installation and facing towards the cardinal directions.

Keywords: organic photovoltaic (OPV); performance analysis; energy efficiency; irradiance and temperature behavior

check for updates

Citation: Dolara, A.; Leva, S.; Manzolini, G.; Simonetti, R.; Trattenero, I. Outdoor Performance of Organic Photovoltaics: Comparative Analysis. *Energies* **2022**, *15*, 1620. https://doi.org/10.3390/en15051620

Academic Editors: Vincenzo d'Alessandro, Pierluigi Guerriero and Frede Blaabjerg

Received: 10 January 2022
Accepted: 17 February 2022
Published: 22 February 2022

Publisher's Note: MDPI stays neutral with regard to jurisdictional claims in published maps and institutional affiliations.

Copyright: © 2022 by the authors. Licensee MDPI, Basel, Switzerland. This article is an open access article distributed under the terms and conditions of the Creative Commons Attribution (CC BY) license (https://creativecommons.org/licenses/by/4.0/).

1. Introduction

Organic photovoltaics (OPVs) are considered one of the most promising technologies for solar energy conversion into electricity, mainly thanks to the reduced cost of manufacturing as well as environmental impact, semi-transparency, low weight, flexibility, and the possibility of modifying the color and the shape of cells [1,2]. Moreover, the late-stage customization process allows to conform OPV modules to any form or shape [3]. In addition, OPV absorption wavelengths can be tuned by molecular engineering [4]. These specific features create the possibility of using organic photovoltaics in several applications, without compete with traditional PV technologies. Building integration is one of the most promising fields of application such as semi-transparent balustrades and solar urban furniture or facades [5]. In such cases, customization of the product and harmonic integration of the structures are key points for the success of any PV technology.

Currently, there are two main weak points of OPV technology: the power conversion efficiency and the stability of its performance over its life and in terms of its irradiance and temperature. The power conversion efficiency—for cell and/or OPVs of limited size—has increased, reaching the current certified value of 17.1% for single-junction cells [6] and above 17% for multi-junction devices [7]. The measured electrical efficiency of OPV modules in outdoor conditions is ~4% [8], although some very interesting results are obtained for small modules [9].

OPV stability is a complex topic that involves many different aspects [10]: manufacturing processes and materials; environmental sustainability; product safety; efficiency decrease over time due to the device exposure; and absence of visible optical changes such as discoloration and yellowing. In terms of stability, comprehensive analyses are presented in [8–10], where some results of the experimental activities are described. Recent studies show how bulk heterojunction organic photovoltaics [11] and non-fullerene

electron acceptors have led to a step change in performance and reduced the problem linked to poor stability in a relatively short period of time [12]. In addition, a low-band gap poly(benzodithiophene-cothieno[3,4-b]thiophene) (PBDTTT) donor polymer blended with a fullerene acceptor has been introduced to increase the thermal stability in flexible organic photovoltaics [13]. Several works have analyzed OPV modules' outdoor behavior, mainly focusing on behavior as a function of irradiance and temperature as well as cell degradation issues and improvements in their long-term stability [14,15]. Furthermore, in [16], the examination of flexible, semi-transparent, organic photovoltaic modules in an outdoor testing environment to study degradation in a hot, arid climate was presented, showing a large reduction in the power conversion efficiency. In [17], tests on OPV mini-modules in air and without hazardous solvents were conducted to compare their outdoor performance, showing that condensation is a significant stress factor in OPVs and should be considered more prominently in reliability studies.

Long-term reliability as well as the behavior of OPV modules in real environments remain topics that need further investigation and analysis. In addition, most of the works dealing with the performances of OPV modules as a function of the irradiance spectrum and temperature in outdoor conditions are based on single prototypes of OPV cells or small-scale OPV module prototypes [17,18], or experimental campaigns are limited to short observational periods or specific environmental conditions [19].

This paper moves the research target from OPV prototypes to ready-to-install OPV modules. The aims of this paper were (i) to analyze and compare OPV modules' behavior with respect to other PV technologies (i.e., market available mc-Si and CIS modules) at different irradiation levels and ambient temperatures and (ii) to assess of the energy produced by OPV modules vertically installed and facing towards the cardinal directions. Both analyses were based on the measurement of the I–V curves and the back temperature in outdoor conditions. In the present work, ASCA® OPV modules produced by "ASCA—an ARMOR group company, Nantes, France" were tested in outdoor conditions. These OPV modules are one of the first examples of relevant scale that can be considered "advanced prototypes". They are based on the stack structure PET/TCO/ZnO/MBG (Medium band gap) donor: PCBM/PEDOT/PSS/Ag.

This paper is organized as follows: Section 2 describes the experimental setup and tests methodologies; Section 3 provides the results of the comparative analysis between OVPs and other PV technologies and the energy analysis with OPV modules facing towards the cardinal directions; Section 4 presents the conclusions.

2. Experimental Setup and Tests Methodologies

The electrical data from PV modules usually provided by manufactures are the maximum power (P_{mpp}) and its coordinates in the I–V plane (V_{mpp} and I_{mpp}), the open circuit voltage (V_{oc}), and the short circuit current (I_{sc}) in two specific conditions: standard test conditions (STCs; solar irradiance = 1000 W/m^2, cell temperature = 25 °C, and air mass = 1.5) and nominal module operating temperature (NMOT; solar irradiance = 800 W/m^2, ambient temperature = 20 °C, air mass = 1.5, and wind speed = 1 m/s). However, STC is not representative of the actual operating conditions, and also NMOT represents a very specific operating condition: solar irradiance, operating temperature of the cells and air mass change throughout the day [19]. Electrical data from PV modules are temperature and/or irradiance dependent; several methods, which also make use of the temperature coefficients provided by the manufacturer, allow for the calculation of PV electrical parameters for a specific set of solar irradiance and cell temperature [20,21]. These calculations are validated for PV modules based on traditional technologies, such as crystalline silicon, whose behavior as a function of irradiation and temperature is well known. OPV modules belong to an emerging photovoltaic technology characterized by its own temperature and irradiance dependencies; the main purpose of this work was to analyze in detail the behavior of ready-to-market OPV modules under actual operating conditions.

Two outdoor experimental campaigns were designed and carried out at the SolarTech-Lab, located at the Department of Energy of Politecnico di Milano, Milano, Italy (geographical coordinates: latitude 45.503 N, longitude 9.157 E) [22]. The first experimental campaign was designed to analyze the behavior of OPV modules in comparison with other PV technologies under different outdoor conditions, while the second experimental campaign was designed to assess the energy produced by the OPV modules vertically installed and facing towards the cardinal directions, recording the electrical data that characterized their operation. In the following, the materials and methods involved in the experimental campaigns are described.

2.1. Test Facility and Weather Station

The test facility is located on the rooftop of the Department of Energy of Politecnico di Milano. All PV modules were oriented towards the southeast, the azimuth angle was $-6°30'$ (0° was the south direction and counted positive clockwise) with the tilt of most structures set at 30°. The latter pair of angles defined the orientation of the conventional plane of array (*POA*) of the test facility. Moreover, it was possible to install PV modules in the vertical position (tilt = 90°) by fixing them to the railing at the edges of the external part of the laboratory; in this case, four azimuth angles were obtained ($-6°30'$, corresponding to the conventional south; $-96°30'$, corresponding to the conventional east; $+83°30'$, corresponding to the conventional west, and $+173°30'$, corresponding to the conventional north).

The environmental conditions were measured with a meteorological station including solar irradiance sensors, a wind speed/direction sensor, a temperature–humidity sensor, and rain collector. Solar irradiance was measured using spectrally flat pyranometers (see metrological characteristics and orientation in Table 1) and an occultation band. Measurements of the ambient conditions were performed every 10 s.

Table 1. Technical specifications of pyranometers connected to the weather station and available at the test facility.

	Pyra #1	**Pyra #2**	**Pyra #3**
ISO9060 classification	Secondary Standard		First Class
Achievable accuracy (95% confidential level)	±2%		±5%
Nonlinearity % (1000 W/m^2)	<±0.2%		<±1%
Tilt	30°	0°	0°
Azimuth	$-6°30'$	-	-
Measurement	Plane-Of-Array (*POA*)	Global Horizontal Irradiance (*GHI*)	Diffuse Horizontal Irradiance (*DHI*)

2.2. Data Acquisition System

The data acquisition consisted of three main subsystems, controlled and coordinated by a PC, the I–V tracer, the PV module selection system, and the PV module temperature acquisition system. Figure 1 shows the whole data acquisition system in the configuration for the comparison between OPVs and other photovoltaic technologies.

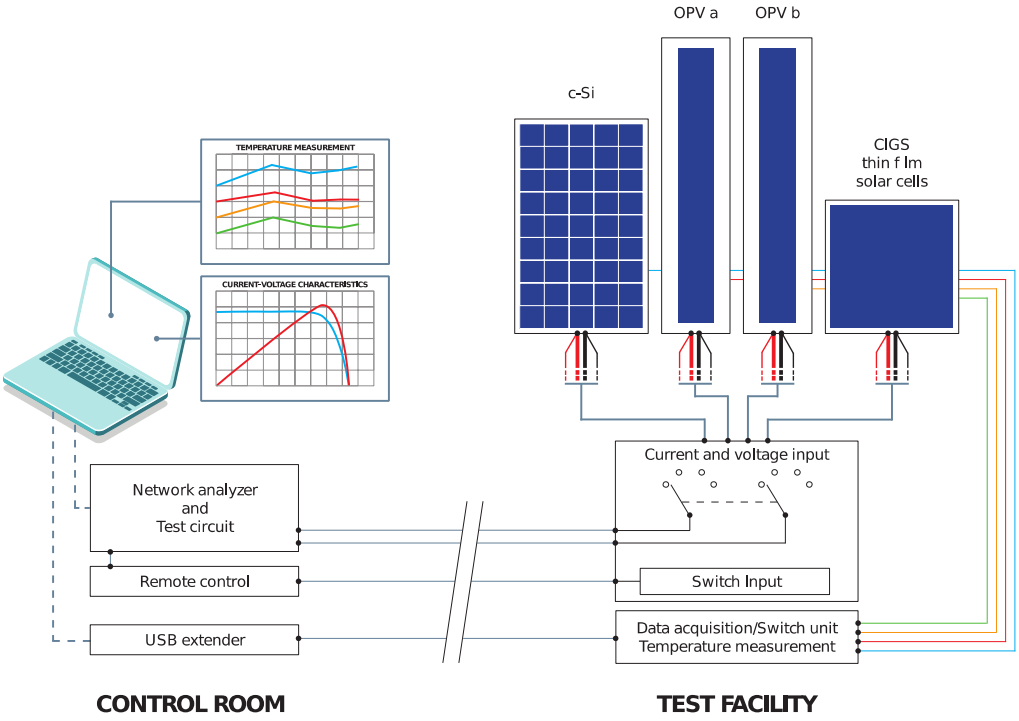

Figure 1. Diagram of the data acquisition system.

The I–V curve tests were performed using the equipment widely described in [8,14]. The I–V curve was traced by charging and discharging a capacitor, the value of which depended on the module under test. To ensure constant irradiance and a constant PV cell temperature along the test, the sampling frequency was set at 12.5 kSamples/s. Considering a recording duration of about 0.5 s, approximately 6000 pairs of samples per test were produced.

To guarantee similar conditions for the tests, an automatic system switched in a short time among the PV modules under test and configured the I–V tracer test circuit with the suitable capacitor.

The PV modules' temperature was measured and managed by an automatic data acquisition system based on a resistance temperature detector (RTD) placed on the back of each PV module. A thermal imaging camera was used to check the temperature uniformity of all of the PV modules and to verify the absence of hotspots.

2.3. OPV Modules

In the present work, ASCA® OPV modules of 17.5 Wp at STCs produced by "ASCA—an ARMOR group company" were tested in outdoor conditions [23].

These OPV modules, which are flexible and semi-transparent, are based on the stack structure PET/TCO/ZnO/MBG (medium band gap) donor: PCBM/PEDOT:PSS/Ag. These OPV modules are inverted devices to achieve a better outdoor stability and make use of a highly conductive transparent conductive layer (TCO) to allow wider stripe coatings and geometrical fill factor (GFF) optimization. Layers from the ETL to the silver top electrode are solution processed.

The OPV modules were ready for installation in PV plants. They included a bypass diode and cables with MC4 connectors. The mechanical support was an aluminum plate where the OPV modules were pasted on by the adhesive layer on the back of each OPV module.

Five OPV modules, divided into two subsets, were involved in the test campaigns. Two OPV modules, hereinafter referred to as OPV-A and OPV-B, were used for the comparison between OPVs and traditional PV technologies, and three OPV modules, hereinafter referred to as OPV-E, OPV-S, and OPV-W, were used for the evaluation of the OPV modules' power generation potential in vertical installation when pointing at different cardinal directions.

2.4. Comparison between OPVs and Traditional Photovoltaic Technologies

The aim of this test campaign was (i) to assess how the main parameters that characterize the operation of OPV modules, namely, V_{oc}, I_{sc}, V_{mpp}, I_{mpp}, and P_{mpp}, changed during operation in outdoor conditions; (ii) to compare these results with those obtained with traditional PV technologies, namely, mc-Si and CIS, in the same outdoor conditions. The comparative analysis of the OPV technology performance with mc-Si PV and CIS was based on the measurement of the I–V curves and the back temperature at different irradiation levels and ambient temperatures. This experimental campaign started on 12 February 2020, and it lasted for approximately four months to collect I–V curves along different seasons. Two OPV modules, the monocrystalline module (Aleo Solar S59 HE, rated power 305 Wp, hereinafter referred to as mc-Si) and the CIS module (Solar Frontier, SF170-S, rated power 170 W, hereinafter referred to as CIS) were installed on the same 30° tilted structure, facing 6°30′ towards the southeast as shown in Figure 2.

Figure 2. PV modules for comparative analysis among PV technologies. From left to the right: monocrystalline silicon, OPVs, and CIS.

The PV technology comparison was achieved following a two-step approach: the whole set of data was divided into five groups based on irradiance level (i.e., <200, 200–400, 400–600, 600–800, and >800 W/m^2) and then the proper per-unit values of V_{oc}, I_{sc}, V_{mpp}, I_{mpp}, and P_{mpp} were calculated for the considered PV technologies. The first step allowed for the selection and comparison of the results obtained under similar irradiance conditions, while the last step allowed for the representation of the results from different PV technologies in a consistent framework. The relative open circuit voltage (v_{oc}) and the relative maximum power point voltage (v_{mpp}) were calculated as follow:

$$v_{oc} = \frac{V_{oc}}{V_{oc@STC}}; \quad v_{mpp} = \frac{V_{mpp}}{V_{mpp@STC}} \tag{1}$$

The base values were V_{oc} and V_{mpp} at STCs. Since I_{sc}, I_{mpp}, and P_{mpp} depend on the irradiance, it is necessary to refer to the raw data of a specific irradiance value; in this work, the average irradiance of each data cluster (G_{REF}) was adopted. Then, the values of I_{sc}, I_{mpp}, and P_{mpp} corrected to irradiance G_{REF}, namely, $I_{sc@Gref}$, $I_{mpp@Gref}$, and $P_{mpp@Gref}$, were reported in per unit. The base values were I_{sc}, I_{mpp}, and P_{mpp} at STCs corrected to irradiance G_{REF}, respectively. Linear correction for both the measured and reference values of I_{sc},

I_{mpp}, and P_{mpp} were applied; then, the equations for the calculation of relative short circuit current ($i_{sc@Gref}$), relative maximum power point current ($i_{mpp@Gref}$), and relative maximum power ($p_{mpp@Gref}$) corrected to irradiance G_{REF} are:

$$i_{sc@G_{ref}} = \frac{I_{sc}}{I_{sc@STC}} \cdot \frac{G_{STC}}{G}; \quad i_{mpp@G_{ref}} = \frac{I_{mpp}}{I_{mpp@STC}} \cdot \frac{G_{STC}}{G}; \quad p_{mpp@G_{ref}} = \frac{P_{mpp}}{P_{mpp@STC}} \cdot \frac{G_{STC}}{G} \tag{2}$$

where G is the actual irradiance, and G_{STC} is 1000 W/m^2.

In order to identify the actual reference electrical data for each PV module involved in the test campaign, outdoor tests were performed under close to STCs in terms of both irradiance and cell temperature at the beginning and at the end of the test campaign. In order to obtain reference electrical data referring to the same conditions, they were corrected to the reference irradiation of 1000 W/m^2. Table 2 summarizes the reference data resulting from the outdoor tests at STCs.

Table 2. Reference electrical data in STCs for the four PV modules compared.

Quantity	Unit	m-Si	CIS	OPV-A	OPV-B
P_{mpp}	(W)	301.1	171.1	19.86	19.81
V_{mpp}	(V)	31.9	88.8	11.9	12.0
I_{mpp}	(A)	9.44	1.93	1.67	1.65
V_{oc}	(V)	39.4	114.3	16.2	16.5
I_{sc}	(A)	9.98	2.12	2.10	2.06

2.5. OPV Modules' Power Generation Potential in Vertical Installation

The aim of this test campaign was to assess the power generation potential of OPV modules vertically installed, as in building-integrated PV applications. In a similar way to the comparative analysis among OPV and other PV technologies, the assessment of the energy produced by the OPV modules vertically installed and facing towards the cardinal directions was based on the measurement of the I–V curves and the back temperature of the PV modules under test. Two OPV modules were installed on the edge of the test facility, facing south (OPV-S) and west (OPV-W) and connected to the data acquisition system. Figure 3 shows the OPV modules installed on the edge of the test facility, and Figure 4 shows the details of OPV-W; OPV-S was installed in the same way.

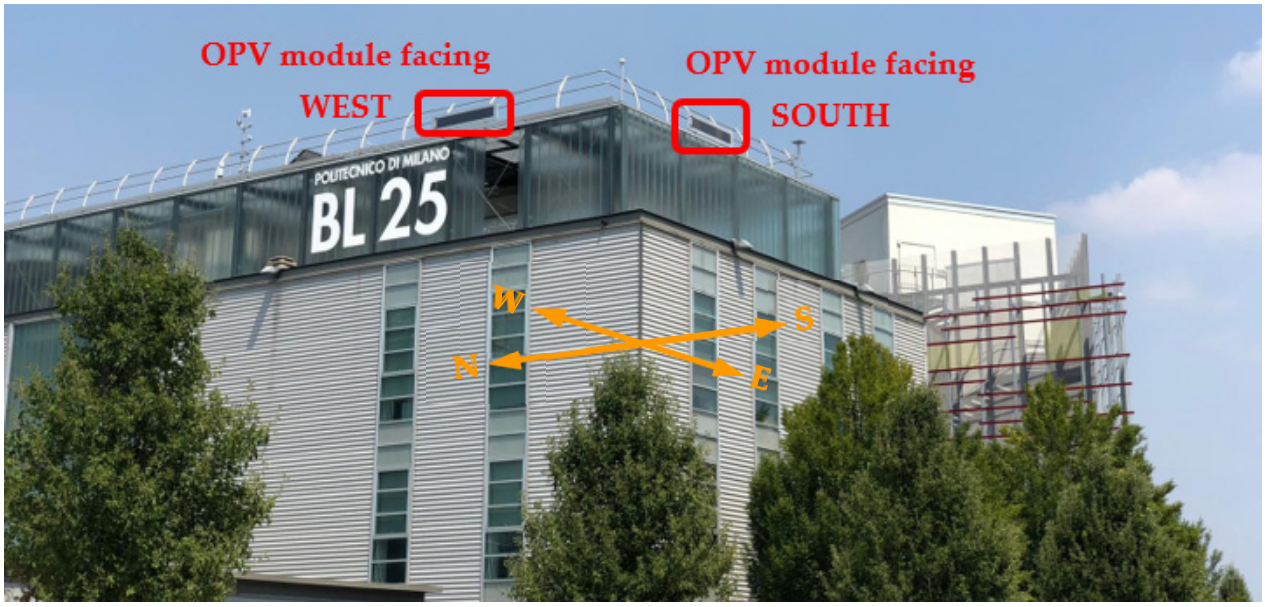

Figure 3. OPV modules installed at the SolarTechLab. The cardinal directions are indicated qualitatively.

Figure 4. OPV module facing west (OPV-W) installed at the edge of the test facility.

This experimental campaign started on 10 October 2020 and lasted for approximately five months. During the testing period, 15 days were selected to assess the OPV power generation potential in different seasons and on different days from a meteorological point of view. The I–V curves of the OPV modules were measured at regular intervals, about every three minutes, throughout the selected days. The daily OPV module power generation curves were estimated from the measured maximum power. Then, the energy production was estimated as the time integral of the maximum power extracted from the I–V curves in a specific time range, as explained below, and daily energy yield (Y_A), daily reference yield (Y_R), and daily performance ratio (PR) [22,24] were chosen to summarize the energy production of the OPV modules. Moreover, Y_A, Y_R, and PR were calculated based on the overall data set, which spanned 15 days.

Compared to the connection of the OPV module with a power converter programmed to operate at the module maximum power point, this methodology had the following benefits:

- A maximum power point tracking (MPPT) algorithm was not necessary: the results related to the maximum power point (i.e., P_{mpp}, V_{mpp}, and I_{mpp}) were not affected by the tracker accuracy;
- Data corresponding to partial shading were uniquely identified, then excluded from the data set;
- V_{oc} and I_{sc} were also available and derived from the I–V curve;
- I–V curve measurements were carried out with the same instrument: the measurement accuracy was the same for every I–V curve of the data set.

The metrics chosen to summarize the energy production of the OPV modules require the definition of a proper time range and the calculation of the global irradiance on the planes of the OPV modules. The setting of the time range for the calculation of the daily production and performance indices was based on the following procedure:

- Step 1: The samples corresponding to the absence of partial shading, due to the nearby buildings close to the test facility, on both OPV modules were extracted from the raw data;
- Step 2: The lower and upper boundaries of the time range for the metrics calculation were defined so that the central value of the range corresponded with the time when OPV-W started to receive direct irradiance. This instant corresponds to a few minutes before solar noon due to the slight eastward orientation of the laboratory.

Step 2 aims to define an "equivalent day" capable of emphasizing the role of orientation in the cardinal directions of the OPV modules, taking into account the same number of morning hours as afternoon hours for the OPV modules' operation analysis.

The irradiance on the planes of the OPV modules was calculated starting from the measurements of the weather station. The horizontal plane beam component was calculated as the difference between *GHI* and *DHI*; the direct normal irradiance (*DNI*) was calculated taking into account the angle of incidence between solar beams and irradiance sensors (ϑ_{bs}):

$$DNI = \frac{GHI - DHI}{\cos(\vartheta_{bs})} \tag{3}$$

For both OPV modules, the global irradiance was calculated as the sum of the beam and the diffuse components on the plane of each OPV; the first one was calculated by adjusting *DNI* by the angle of incidence between solar beams and the plane of each OPV (ϑ_{bm}); the latter was calculated by using the isotropic sky diffuse model.

$$G_{OPV} = DNI \cdot \cos(\vartheta_{bm}) + DHI \cdot \frac{1 + \cos(\vartheta_T)}{2} \tag{4}$$

In vertical installation, the tilt angle, ϑ_T, was 90°. The ground-reflected irradiance on the planes of the OPV modules was negligible due to the particular installation conditions that characterized the test facility. This calculation methodology was validated with the measurements of the irradiance on the planes of the OPV modules obtained with a portable irradiance meter as shown in Figure 4. This last instrument cannot be used along the entire measurement campaign due to the limited internal memory.

3. Results

3.1. Comparison between OPVs and Traditional Photovoltaic Technologies

The row data obtained during the test campaign concerning the comparison between OPVs and traditional photovoltaic technologies were processed as described in Section 2.5. The results are presented in the scatterplots organized as follows: Figure 5 shows the relative V_{oc} and the relative I_{sc} as a function of the module temperature; Figure 6 shows the relative coordinates in the I–V plane of the maximum power point as a function of the module temperature; Figure 7 shows the resulting relative maximum power. The least squares method was chosen to estimate the temperature coefficients by fitting the data in each irradiance range and for each electrical data.

Concerning V_{oc} as a function of the cells' temperature (see Figure 5), the mc-Si and CIS modules showed a linear decrease with the cells' temperature, while the OPV modules had a quite constant V_{oc} for any cell temperature in all the considered irradiance ranges. In detail, the temperature coefficient of V_{oc} for mc-Si and CIS almost coincided for all data clusters with an irradiance above 400 W/m^2 and they have been estimated to be −0.29%/K for mc-Si and −0.22%/K for CIS, as expected from the rated temperature coefficient reported in their datasheets. At lower irradiance values, the estimated temperature coefficient of V_{oc} dropped to an average value of approximately −0.20%/K for both mc-Si and CIS. However, the limited amount of data for these irradiation ranges increased the uncertainty related to the estimated value of the temperature coefficient. These results also allow for the validation of the measurement system and the data processing procedure: the reference temperature coefficient of V_{oc} for mc-Si was −0.29%/K, which is exactly the same as estimated. Differently from the mc-Si and CIS, the OPV modules had a quite constant V_{oc} in all irradiance ranges: slightly increasing with the cell temperature at irradiance values below 400 W/m^2 and barely decreasing with the cell temperature for higher irradiance values. In all irradiance ranges, the absolute values of the temperature coefficient of V_{oc} were always below 0.05%/K. The same result was also found [19] at two specific irradiance values and in a narrower temperature range compared to the present work. This result is peculiar to some of the OPV materials.

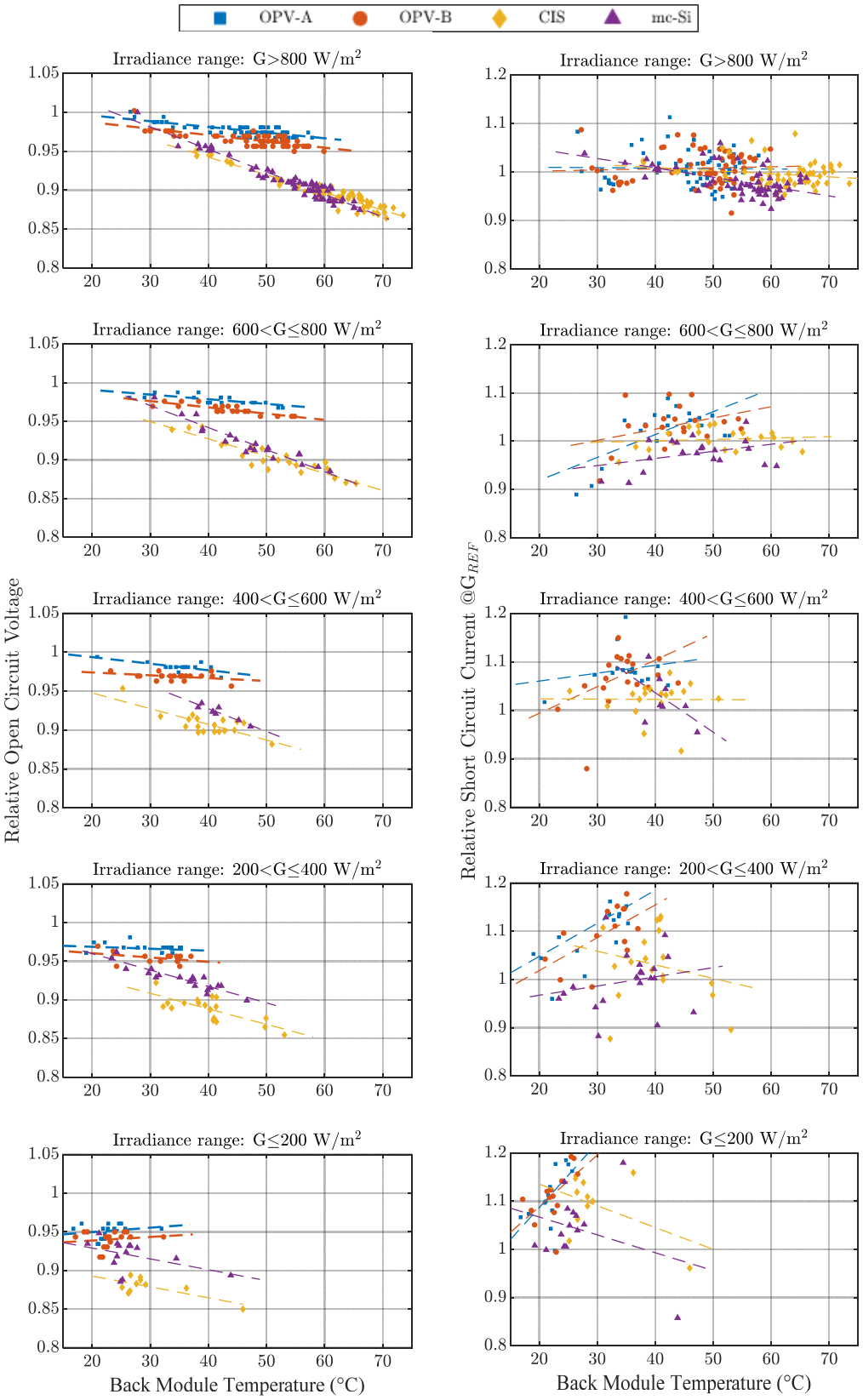

Figure 5. Relative open-circuit voltage (**a**) and relative short-circuit current (**b**) as a function of the back module temperature for the whole set of PV modules under test.

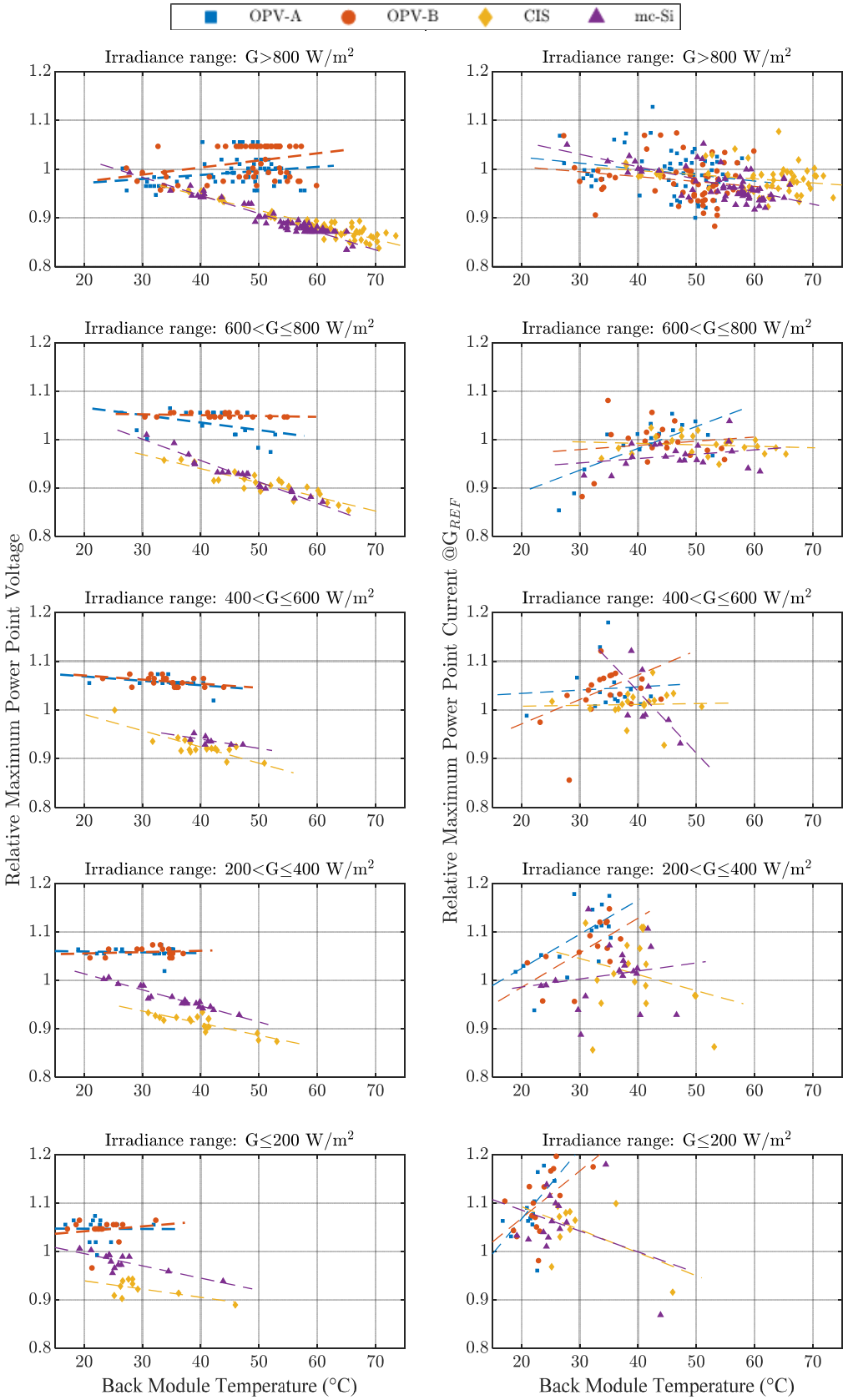

Figure 6. Relative maximum power point voltage (**a**) and relative maximum power point current (**b**) as a function of the back module temperature for the whole set of PV modules under test.

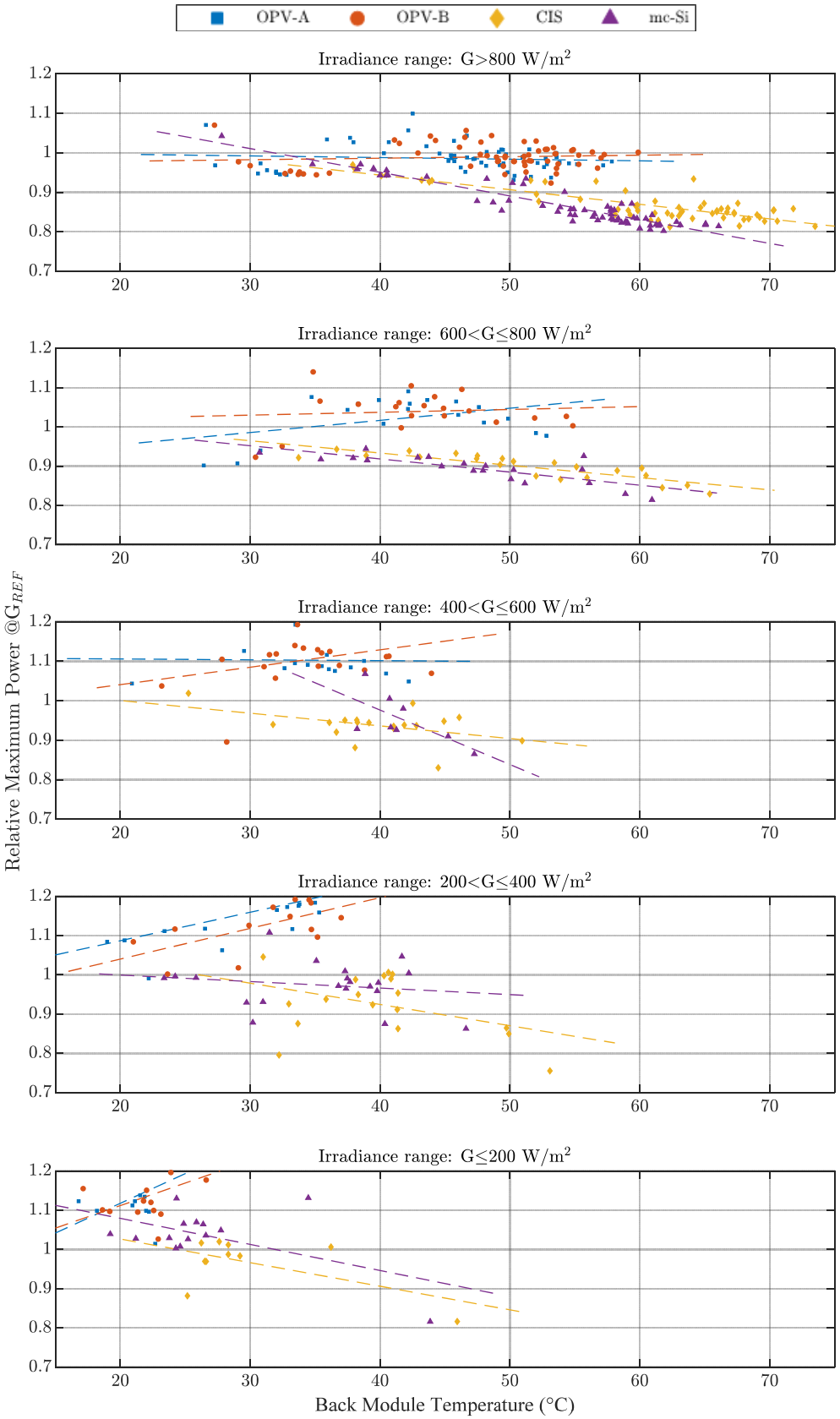

Figure 7. Relative maximum power as a function of the back module temperature for the whole set of PV modules under test.

Concerning I_{sc} as a function of the cells' temperature (see Figure 5), mc-Si and CIS technologies showed similar and almost constant behavior, while the expected behavior should be a slightly increasing linear trend (+0.05%/K for mc-Si and +0.01%/K for CIS, as expected from the rated temperature coefficient reported in their datasheets). This discrepancy is related to the intrinsic uncertainty of outdoor measurements as atmospheric conditions (namely, the solar spectrum) and moisture. The I_{sc} of the OPV modules was quite constant with temperature at high irradiance values (G > 800 W/m^2), while it increased with temperature at lower irradiance values. It must be pointed out that in the lower irradiance range, it was not possible to accurately estimate the temperature coefficient because of the limited amount of data. Differently from other authors [19], the results at high irradiance did not show a slight increase in the short circuit current with the OPV cells' temperature. This may be due to the different approaches during the two measurement campaigns. First of all, the OPV cells tested in [19] were not based on the same materials. Moreover, in [19], a narrow temperature range of approximately 15 °C were considered for two specific irradiance values (i.e., 600 and 1000 W/m^2); in this work, the irradiance values varied between 100 and 1000 W/m^2 and the cell temperature in a wider temperature range of approximately 40 °C. Finally, the test campaign in [19] was carried out for few days, while this work covered a longer period including three seasons. Compared to the preliminary results presented in [8], the small reduction in I_{sc} seemed to be related to aging along the whole test campaign: the measurements at high temperatures corresponded to the last period of the measurement campaign.

Concerning the coordinates of the MPP, V_{mpp} and I_{mpp}, they had a similar behavior to V_{oc} and I_{sc} as described above (see Figure 6). The mc-Si and CIS modules were characterized by a linear decrease in V_{mpp} with the cell temperature, while I_{mpp} was almost constant. The temperature coefficients of V_{mpp} for mc-Si and CIS were similar to those found for V_{oc} in any irradiance range. On the contrary, OPVs showed a slightly increasing V_{mpp} with the cell temperature at high irradiance, while it was almost constant with the cell temperature for irradiance values below 800 W/m^2. OPV-A and OPV-B had quite different temperature coefficients of V_{mpp} for irradiance values higher than 600 W/m^2. The I_{sc} of the OPVs had a slightly decreasing trend with temperatures at high irradiance (G > 800 W/m^2) and an increasing trend with temperature at lower irradiance values. Differences between the slopes of the trend lines obtained for OPV-A and OPV-B, in particular between 400 and 800 W/m^2, were mainly due to the small amount of data in the corresponding irradiance ranges and may partly be related to the different aging processes of the "advanced prototypes" of OPV modules involved in this test campaign.

The maximum power changed with the temperature as result of the product of V_{mpp} and I_{mpp} (see Figure 7). The mc-Si and CIS modules were characterized by a linear decrease in P_{mpp} with the cell temperature, with a similar slope in each irradiance range as expected from the rated temperature coefficient reported in their datasheets. The OPV modules showed a quite constant P_{mpp} with the cell temperature for irradiance values higher than 800 W/m^2 and an increasing P_{mpp} at lower irradiance values. In the higher irradiance range, the slight decrease in V_{mpp} balanced the slight increase in I_{mpp} with the cell temperature resulting in a constant P_{mpp}. In irradiance ranges lower than 800 W/m^2, the maximum power increase was mainly related to the increase in I_{mpp}. No direct comparison of these results with the one available in literature could be performed. The average conversion efficiency was similar to those found in [17,18] at the beginning of the test campaigns and similar to that found in [19].

3.2. OPV Modules' Power Generation Potential in Vertical Installation

The raw data obtained during the test campaign concerning the assessment of the energy produced by the OPV modules vertically installed and facing towards the cardinal directions were processed as described in Section 2.5.

Figure 8 summarizes the weather conditions on each considered day. Raw data corresponding to a sunny day are reported in Figures 9–12 showed the same raw data corresponding to a cloudy day, while Figures 13 and 14 corresponded to a partially cloudy

day. Table 3 shows the metrics that summarize the daily energy production. For all the figures, the solid line with markers corresponds to the data set selected to calculate production yields and performance index, while the dashed line represents the raw data that have been excluded from the analysis. Moreover, the black dotted line corresponding to *GHI* gives quite general information about the irradiance available along each day.

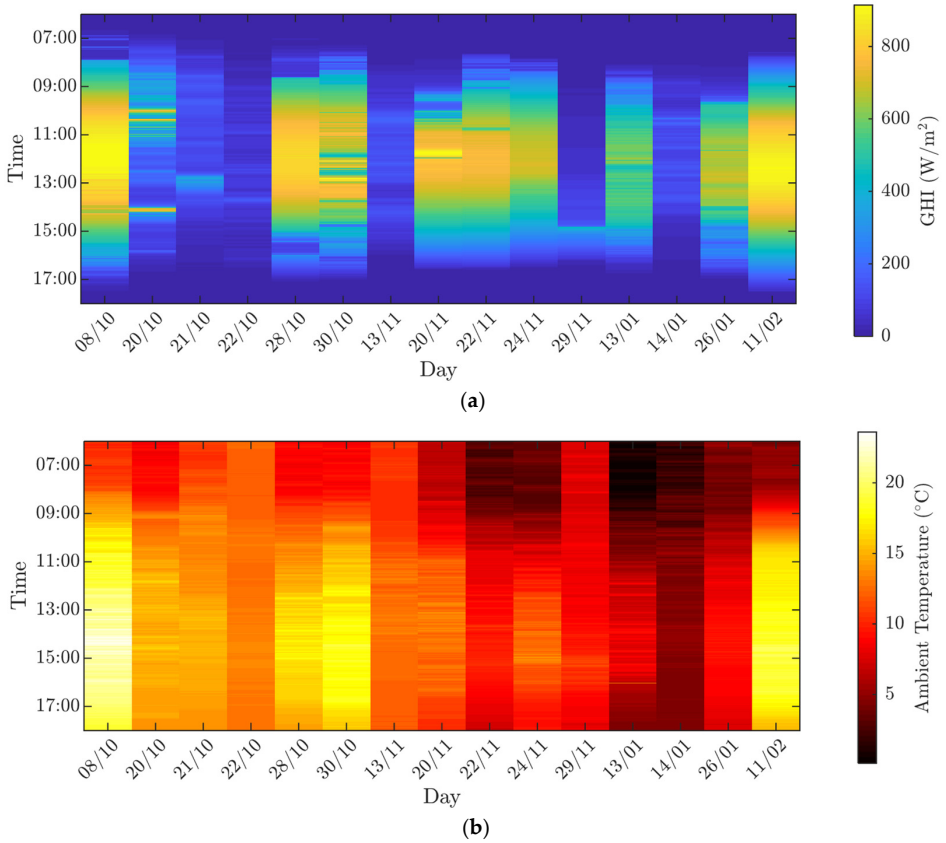

Figure 8. Weather conditions during the test campaign: (**a**) *GHI*; (**b**) ambient temperature.

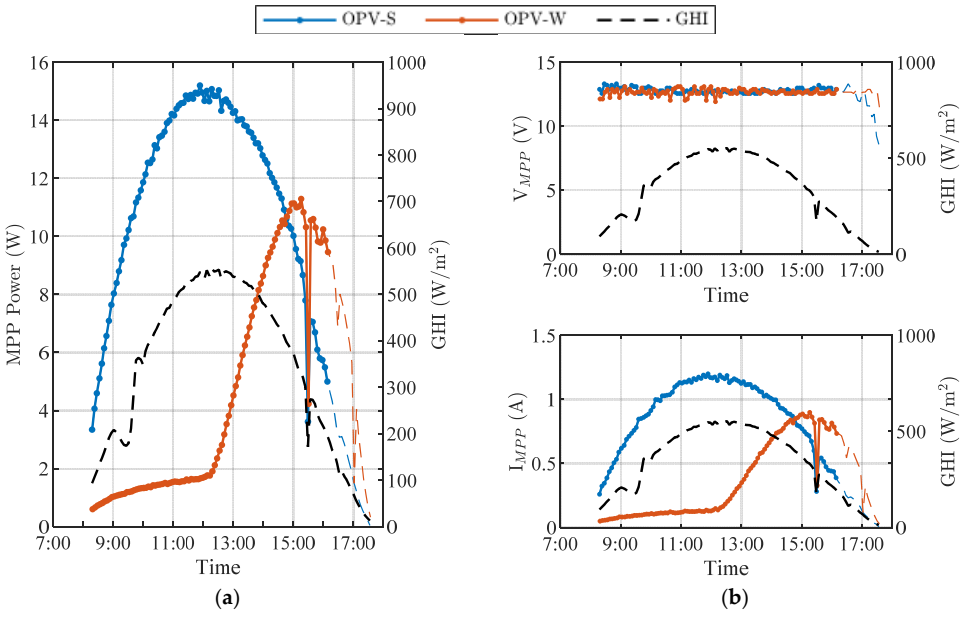

Figure 9. Example of raw data on a sunny day: (**a**) maximum power, P_{mpp}; (**b**) its coordinates, V_{mpp} and I_{mpp}, recorded on 11 February 2021.

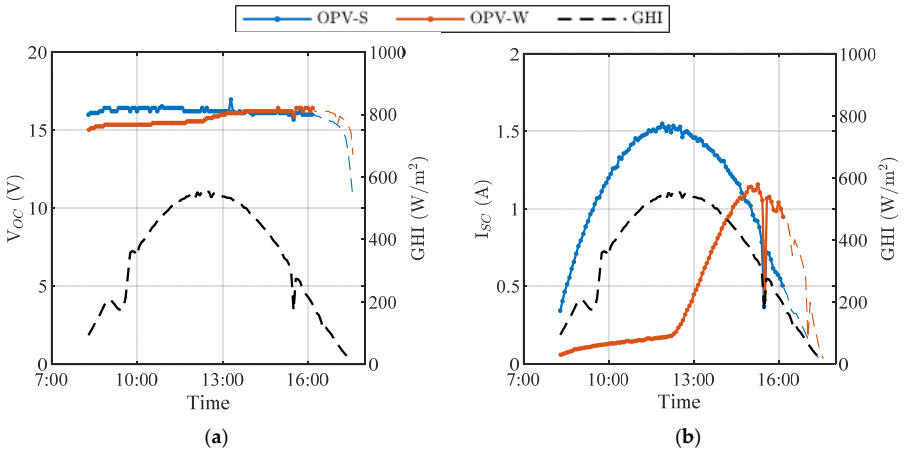

Figure 10. Example of raw data on a sunny day: (**a**) open-circuit voltage, V_{oc}; (**b**) short-circuit current, I_{sc}, recorded on 11 February 2021.

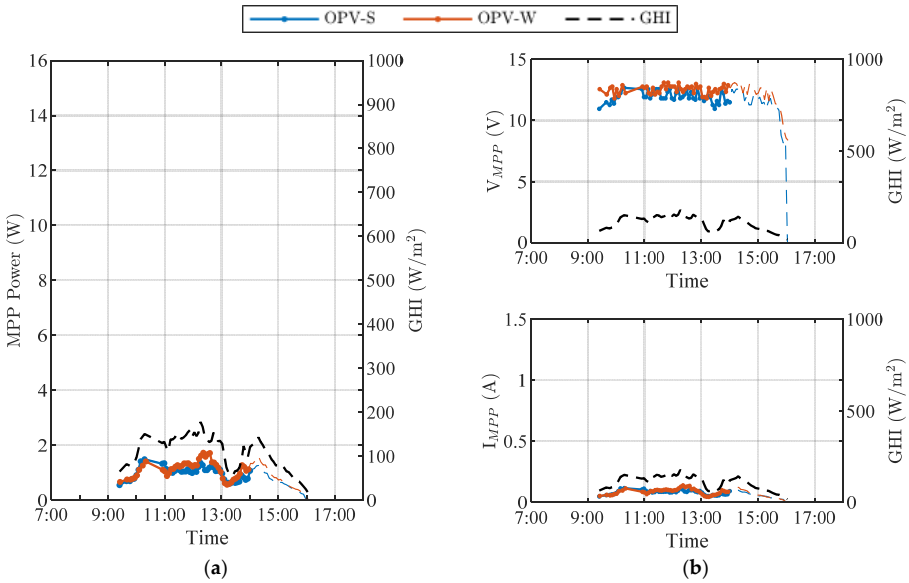

Figure 11. Example of raw data on a cloudy day: (**a**) maximum power, P_{mpp}; (**b**) its coordinates, V_{mpp} and I_{mpp}, recorded on 13 November 2020.

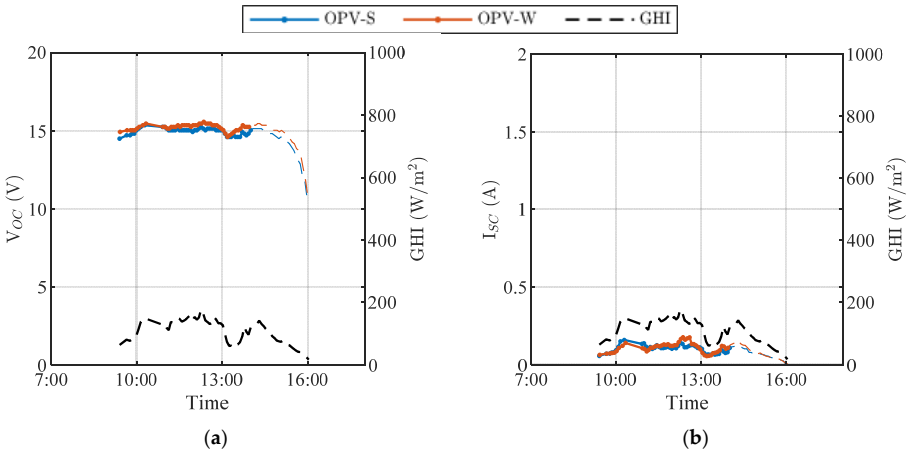

Figure 12. Example of raw data on a cloudy day: (**a**) open-circuit voltage, V_{oc}; (**b**) short-circuit current, I_{sc}, recorded on 13 November 2020.

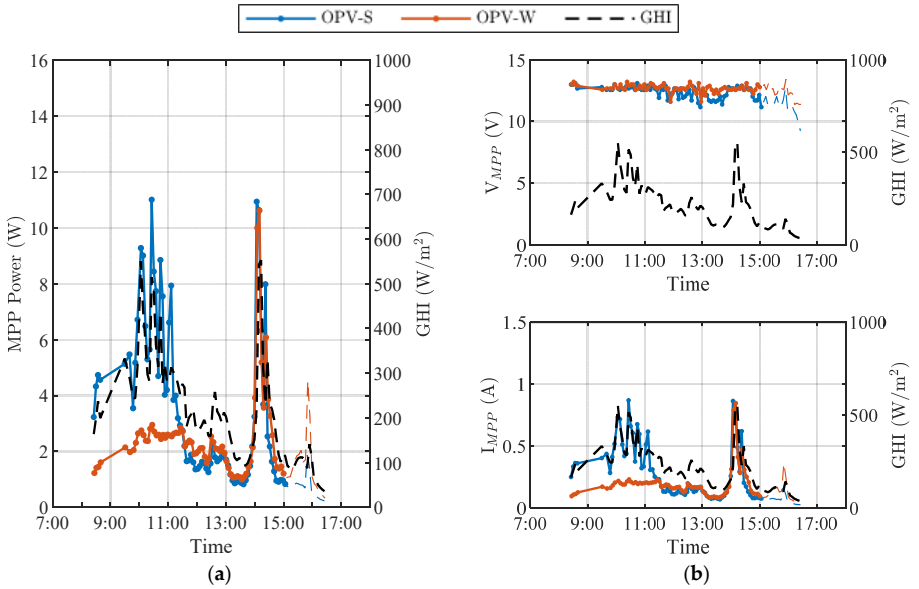

Figure 13. Example of raw data on a partially cloudy day: (**a**) maximum power, P_{mpp}; (**b**) its coordinates, V_{mpp} and I_{mpp}, recorded on 11 February 2021.

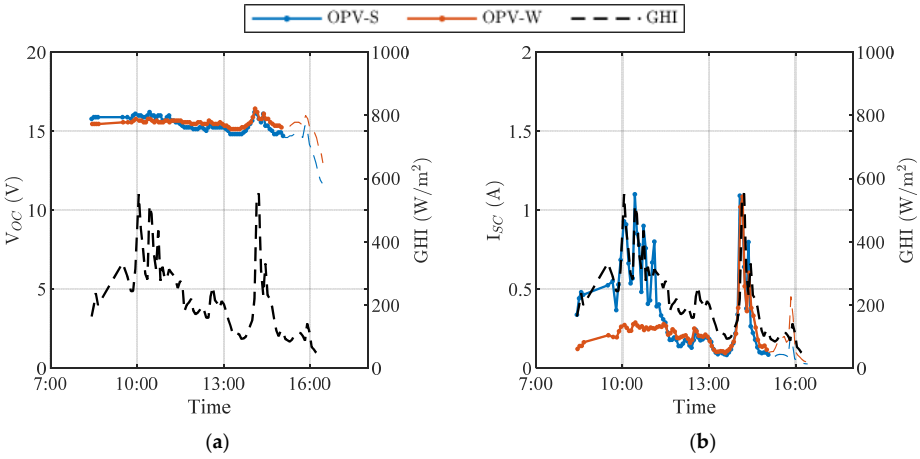

Figure 14. Example of raw data on a partially cloudy day: (**a**) open-circuit voltage, V_{oc}; (**b**) short-circuit current, I_{sc}, recorded on 11 February 2021.

As before, the daily recording started at approximately one hour after sunrise and ended at sunset. The delayed start of the recordings was due to the nearby building located eastward from the test facility, shadowing the OPV modules early in the morning.

During sunny days, the *PR* of the OPV-S was higher than the *PR* of the OPV-W, while during cloudy days, this difference disappeared. OPV-S received global irradiance for the whole day, while OPV-W received global irradiance for half of every sunny day, and only diffuse irradiance for the other half of the same day. Taking into account the whole set of days, the *PR* of OPV-S was higher than the *PR* of OPV-W by 4%; this specific value depends on the mix of days present in the data set, suggesting that the OPV modules had a higher conversion efficiency under direct irradiance.

Measurement of the modules' electric characteristics (i.e., V_{oc} and V_{mpp}, I_{sc}, and I_{mpp}) confirmed the results presented in Section 3.1. The maximum power point voltage, V_{mpp}, was almost constant and close to 13 V throughout each day; only operations at extremely low irradiance led to small reductions in V_{mpp}. In the first approximation, the voltage corresponding to the maximum power point did not dependent on temperature and irradiance. This property simplifies the maximum power point tracking: even the simplest

algorithm that keeps the voltage at the terminals of the PV module constant can lead to good conversion efficiencies. Similarly, the open-circuit voltage, V_{oc}, was almost constant with the temperature, but its value depended on the mix of beam and diffuse components of the irradiance: V_{oc} was close to 16 V when the solar beams hit the plane of each OPV, and V_{oc} was reduced to approximately 15 V when only diffuse irradiance was present.

Table 3. Y_R, Y_A, and PR for the two OPV modules under test.

Day	Type [1]	OPV-S			OPV-W		
		Y_R (h)	Y_A (h)	PR (%)	Y_R (h)	Y_A (h)	PR (%)
2020/10/08	S	4.69	4.11	87.6%	2.12	1.63	76.6%
2020/10/20	P	1.48	1.22	82.5%	0.73	0.76	104.7%
2020/10/21	P	0.68	0.48	70.3%	0.48	0.44	92.3%
2020/10/22	C	0.30	0.20	68.0%	0.22	0.22	101.4%
2020/10/28	S	2.87	2.41	84.2%	0.77	0.52	67.7%
2020/10/30	S	3.19	2.83	88.6%	1.29	0.91	70.3%
2020/11/13	C	0.40	0.23	56.9%	0.26	0.25	93.9%
2020/11/20	S	3.71	3.01	81.2%	1.30	1.08	82.6%
2020/11/22	S	3.32	2.61	78.8%	0.94	0.63	66.5%
2020/11/24	S	4.22	3.18	75.3%	1.56	1.08	69.3%
2020/11/29	C	0.20	0.11	55.0%	0.14	0.12	84.9%
2021/01/13	S	5.38	3.99	74.1%	1.87	1.35	72.6%
2021/01/14	P	3.84	3.05	79.2%	1.12	0.80	71.2%
2021/01/26	S	5.18	3.85	74.3%	1.69	1.17	69.2%
2021/02/11	S	5.45	4.39	80.6%	2.33	1.75	75.0%
Whole period		44.92	35.68	79.4%	16.82	12.69	75.4%

[1] Summarizes the weather conditions: S = sunny day; C = cloudy day; P = partially cloudy day.

4. Conclusions

This paper presented the results of two outdoor experimental campaigns performed to (i) evaluate and compare the OPV modules' performance at different irradiation levels and different ambient temperatures with traditional PV technologies and (ii) to assess their power generation potential under different solar radiation conditions. Both test campaigns made use of one of the first of a kind relevant scale OPV modules that, even at this developmental stage, showed different peculiarities compared to conventional PV technologies.

Concerning the operation at different cell temperatures and constant irradiance, the OPV modules showed a quite constant V_{mpp} and an increasing I_{mpp} with the cell temperature, resulting in an increasing P_{mpp} with the cell temperature. On the contrary, the mc-Si and CIS PV modules linearly reduced their maximum power output with the cell temperature, mainly due to the linear decrease in V_{mpp}, while I_{mpp} was almost constant.

Regarding the energy measurements of the vertically installed OPV modules, the OPV module facing south (OPV-S) presented a PR higher than the OPV module facing west (OPV-W) during sunny days, while for cloudy days, the PRs of both OPV modules were similar. This confirms a higher conversion efficiency for the OPV modules under direct irradiance but also a good capability of the OPV modules in converting diffuse irradiance.

Future developments of this work will extend the experimental investigation to a PV generator scale including the issues related to partial shading and hot spots. Moreover, the impact of the aging of the OPV modules and their long-term stability deserve to be experimentally evaluated.

Author Contributions: Conceptualization and methodology A.D. and R.S.; validation, formal analysis, and investigation, A.D., I.T. and R.S.; resources and data curation, A.D. and S.L.; writing—original draft preparation, A.D. and S.L.; writing—review and editing, A.D. and S.L.; supervision, project administration, and funding acquisition, S.L. and G.M. All authors have read and agreed to the published version of the manuscript.

Funding: This research was funded by ENI S.p.A. (Italy). The Authors gratefully acknowledge ENI S.p.A. (Italy) for financial support.

Institutional Review Board Statement: Not applicable.

Informed Consent Statement: Not applicable.

Data Availability Statement: The data presented in this study are available in article.

Conflicts of Interest: The authors declare no conflict of interest.

References

1. Brabec, C.J. Organic photovoltaics: Technology and market. *Sol. Energy Mater. Sol. Cells* **2004**, *83*, 273–292. [CrossRef]
2. Gambhir, A.; Sandwell, P.; Nelson, J. The future costs of OPV—A bottom-up model of material and manufacturing costs with uncertainty analysis. *Sol. Energy Mater. Sol. Cells* **2016**, *156*, 49–58. [CrossRef]
3. Subramaniam, S.V.; Van Der Wiel, B.; Sauermann, T.; Kutsarov, D.; Schilinsky, P.; Patzold, R.; Baumann, R.R.; Meier, S.B. Late-Stage Customization in Volume Production of Organic Photovoltaics. *ACS Appl. Electron. Mater.* **2020**, *2*, 756–762. [CrossRef]
4. Scharber, C.; Sariciftci, N.S. Efficiency of bulk-heterojunction organic solar cells. *Prog. Polym. Sci.* **2013**, *38*, 1929–1940. [CrossRef] [PubMed]
5. ASCA Projects. Available online: https://en.asca.com/projects/ (accessed on 9 December 2021).
6. Meng, L.; Zhang, Y.; Wan, X.; Li, C.; Zhang, X.; Wang, Y.; Ke, X.; Ziao, Z.; Ding, L.; Xia, R.; et al. Organic and solution-processed tandem solar cells with 17.3% efficiency. *Science* **2018**, *361*, 1094–1098. [CrossRef] [PubMed]
7. Zhan, L.; Li, S.; Lau, T.; Cui, Y.; Lu, X.; Shi, M.; Li, C.; Li, H.; Hou, J.; Chen, H. Over 17% efficiency ternary organic solar cells enabled by two non-fullerene acceptors working in an alloy-like model. *Energy Environ. Sci.* **2020**, *13*, 635–645. [CrossRef]
8. Dolara, A.; Di Fazio, G.; Leva, S.; Manzolini, G.; Simonetti, R.; Terenzi, A. Outdoor Assessment and Performance Evaluation of OPV Modules. *IEEE J. Photovolt.* **2021**, *11*, 391–399. [CrossRef]
9. Distler, A.; Brabec, C.J.; Egelhaaf, H.J. Organic photovoltaic modules with new world record efficiencies. *Prog. Photovol Res. Appl.* **2021**, *29*, 24–31. [CrossRef]
10. Subramaniam, S.V.; Kutsarov, D.; Sauermann, T.; Meier, S.B. Commercialization of Organic Photovoltaics and Its Product Integration: A Perspective Focusing on Durability. *Energy Technol.* **2020**, *8*, 2000234. [CrossRef]
11. Lee, H.; Park, C.; Sin, D.H.; Park, J.H.; Cho, K. Recent Advances in Morphology Optimization for Organic Photovoltaics. *Adv. Mater.* **2018**, *30*, 1800453. [CrossRef] [PubMed]
12. Meredith, P.; Li, W.; Armin, A. Nonfullerene Acceptors: A Renaissance in Organic Photovoltaics? *Adv. Energy Mater.* **2020**, *10*, 2001788. [CrossRef]
13. Xu, X.; Fukuda, K.; Karki, A.; Park, S.; Kimura, H.; Jinno, H.; Watanabe, N.; Yamamoto, S.; Shimomura, S.; Kitazawa, D.; et al. Thermally stable, highly efficient, ultraflexible organic photovoltaics. *Proc. Natl. Acad. Sci. USA* **2018**, *115*, 4589–4594. [CrossRef] [PubMed]
14. Magadley, E.; Teitel, M.; Peretz, M.F.; Kacira, M.; Yehia, I. Outdoor behaviour of organic photovoltaics on a greenhouse roof. *Sustain. Energy Technol. Assess.* **2020**, *37*, 100641. [CrossRef]
15. Katz, E.A.; Gevorgyan, S.; Orynbayev, M.S.; Krebs, F.C. Out-door testing and long-term stability of plastic solar cells. *EPJ Appl. Phys.* **2006**, *36*, 307–311. [CrossRef]
16. Chief, M.; Boyer, K.; Simmons-Potter, K. In-situ testing of organic photovoltaic (OPV) modules to examine modes of degradation in an arid-hot climate. In Proceedings of the Organic, Hybrid, and Perovskite Photovoltaics XXI 2020, Online, 24 August–4 September 2020. [CrossRef]
17. Soares, G.A.; David, T.W.; Anizelli, H.; Miranda, B.; Rodrigues, J.; Lopes, P.; Martins, J.; Cunha, T.; Vilaça, R.; Kettle, J.; et al. Outdoor performance of organic photovoltaics at two different locations: A comparison of degradation and the effect of condensation. *J. Renew. Sustain. Energy* **2020**, *12*, 063502. [CrossRef]
18. Josey, D.S.; Nyikos, S.R.; Garner, R.K.; Dovijarski, A.; Castrucci, J.S.; Wang, J.M.; Evans, G.J.; Bender, T.P. Outdoor Performance and Stability of Boron Subphthalocyanines Applied as Electron Acceptors in Fullerene-Free Organic Photovoltaics. *ACS Energy Lett.* **2017**, *2*, 726–732. [CrossRef]
19. Bristow, N.; Kettle, J. Outdoor performance of organic photovoltaics: Diurnal analysis, dependence on temperature, irradiance, and degradation. *J. Renew. Sustain. Energy* **2015**, *7*, 013111. [CrossRef]
20. Dolara, A.; Leva, S.; Manzolini, G. Comparison of different physical models for PV power output prediction. *Solar Energy* **2015**, *119*, 83–99. [CrossRef]
21. *IEC Standard 60891*; Photovoltaic Devices—Procedures for Temperature and Irradiance Corrections to Measured I–V Characteristics. International Electrotechnical Commission (IEC): Geneva, Switzerland, 2010. Available online: https://www.iec.ch/homepage(accessed on 15 July 2021).
22. SolarTechLab. Available online: http://www.solartech.polimi.it/ (accessed on 24 July 2021).

23. ASCA®OPV Modules Producer. Available online: https://en.asca.com/ (accessed on 13 October 2021).
24. *IEC Standard 61724*; Photovoltaic System Performance Monitoring—Guidelines for Measurement, Data Exchange and Analysis. International Electrotechnical Commission (IEC): Geneva, Switzerland, 1998. Available online: https://www.iec.ch/homepage(accessed on 18 July 2021).